

Red Fluorescent Protein pH Biosensor to Detect Concentrative Nucleoside Transport^{*S}

Received for publication, May 8, 2009 Published, JBC Papers in Press, June 3, 2009, DOI 10.1074/jbc.M109.019042

Danielle E. Johnson^{†1,2}, Hui-wang Ai^{§1,3}, Peter Wong^{§4}, James D. Young^{‡5}, Robert E. Campbell[§], and Joseph R. Casey^{‡5,6}

From the [†]Membrane Protein Research Group, Department of Physiology, University of Alberta, Edmonton, Alberta T6G 2H7 and the [§]Department of Chemistry, University of Alberta, Edmonton T6G 2G2, Canada

Human concentrative nucleoside transporter, hCNT3, mediates Na⁺/nucleoside and H⁺/nucleoside co-transport. We describe a new approach to monitor H⁺/uridine co-transport in cultured mammalian cells, using a pH-sensitive monomeric red fluorescent protein variant, mNectarine, whose development and characterization are also reported here. A chimeric protein, mNectarine fused to the N terminus of hCNT3 (mNect.hCNT3), enabled measurement of pH at the intracellular surface of hCNT3. mNectarine fluorescence was monitored in HEK293 cells expressing mNect.hCNT3 or mNect.hCNT3-F563C, an inactive hCNT3 mutant. Free cytosolic mNect, mNect.hCNT3, and the traditional pH-sensitive dye, BCECF, reported cytosolic pH similarly in pH-clamped HEK293 cells. Cells were incubated at the permissive pH for H⁺-coupled nucleoside transport, pH 5.5, under both Na⁺-free and Na⁺-containing conditions. In mNect.hCNT3-expressing cells (but not under negative control conditions) the rate of acidification increased in media containing 0.5 mM uridine, providing the first direct evidence for H⁺-coupled uridine transport. At pH 5.5, there was no significant difference in uridine transport rates (coupled H⁺ flux) in the presence or absence of Na⁺ (1.09 ± 0.11 or 1.18 ± 0.32 mM min⁻¹, respectively). This suggests that in acidic Na⁺-containing conditions, 1 Na⁺ and 1 H⁺ are transported per uridine molecule, while in acidic Na⁺-free conditions, 1 H⁺ alone is transported/uridine. In acid environments, including renal proximal tubule, H⁺/nucleoside co-transport may drive nucleoside accumulation by hCNT3. Fusion of mNect to hCNT3 provided a simple, self-referencing, and effective way to monitor nucleoside transport, suggesting an approach that may have applications in assays of transport activity of other H⁺-coupled transport proteins.

Nucleosides are hydrophilic molecules that require transport proteins to mediate their movement across the plasma membrane (1). Human (h)⁷ nucleoside transport (NT) proteins catalyze the vectorial transport of nucleosides, using either concentrative (C) or equilibrative (E) mechanisms (2). hCNTs use either a Na⁺ or H⁺ gradient to accumulate nucleosides against their concentration gradient, whereas hENTs mediate facilitated diffusion of nucleosides down their concentration gradient (3). Nucleoside transporters also transport anti-cancer and anti-viral drugs, and cellular expression of nucleoside transporters is important in cancer therapy as well as in the treatment of cardiovascular, parasitic, and viral diseases (4, 5).

Members of the SLC28 family of concentrative nucleoside transporters (CNTs) divide into two phylogenetic subfamilies: hCNT1/2 belonging to one subfamily, and hCNT3 to the other (6–8). Cation substitution and charge/flux ratio studies suggest that hCNT1/2 couple the inward movement of nucleoside to the Na⁺ electrochemical gradient with a 1:1 stoichiometry, whereas hCNT3 can couple nucleoside transport to either the Na⁺ gradient (2 Na⁺:1 nucleoside) or a H⁺ gradient (1 H⁺:1 nucleoside) in the absence of Na⁺ (9, 10). The 2:1 coupling ratio of hCNT3 allows it to develop a trans-membrane nucleoside concentration gradient up to 10-fold higher than that of hCNT1 or hCNT2 (9, 11). At pH 5.5, hCNT3 also transports uridine in the presence of Na⁺ with a 2 cation:1 nucleoside stoichiometry, which raises the possibility that 1 H⁺ and 1 Na⁺ may be transported per nucleoside molecule in these conditions (9–12). Up to this point, however, there has been no direct demonstration that hCNT3 can transport H⁺.

Concentrative nucleoside transport has previously been investigated using the *Xenopus laevis* oocyte expression system and both electrophysiology (two-microelectrode voltage clamp technique) and radioisotope flux measurements (6–9, 12). Electrophysiological experiments are advantageous in that they

* This work was supported in part by a Canadian Institutes of Health Research operating grant (to J. R. C.), by financial support from the Canada Foundation for Innovation, the Natural Sciences and Engineering Research Council, and Alberta Ingenuity (to R. E. C.), and by support from the National Cancer Institute of Canada (to J. D. Y.).

[§] The on-line version of this article (available at <http://www.jbc.org>) contains supplemental Figs. S1 and S2.

[†] Both authors contributed equally to this work.

² Supported by an Alberta Heritage Foundation for Medical Research (AHFMR) studentship.

³ Present address: The Scripps Research Institute, La Jolla, CA 92037.

⁴ Supported by the Natural Sciences and Engineering Research Council, undergraduate student research award.

⁵ AHFMR Scientists.

⁶ To whom correspondence should be addressed: Dept. of Physiology, University of Alberta, Edmonton, Alberta T6G 2H7, Canada. Tel.: 780-492-7203; Fax: 780-492-8915; E-mail: joe.casey@ualberta.ca.

⁷ The abbreviations used are: h, human; NT, nucleoside transport protein; C, concentrative; E, equilibrative; mNect.hCNT3, mNectarine fused to the N terminus of hCNT3; EIPA, 5-(N-ethyl-N-isopropyl)amiloride; NHE1, Na⁺/H⁺ exchanger isoform 1; FP, fluorescent protein; RFP, red fluorescent protein; mRFP, monomeric RFP; avGFP, *A. victoria* green fluorescent protein; pK_a, equal to the pH at which the fluorescence is half-maximal in intensity; *Discosoma* RFP, tetrameric *Discosoma* RFP; YFP, yellow FP; enhanced avGFP, enhanced GFP; SGLT1, Na⁺/glucose cotransporter isoform 1; PEPT1/2, proton-dependent oligopeptide transporters isoforms 1/2; MCT1, monocarboxylate transporter isoform 1; PNGaseF, peptidase: N-glycosidase F; MES, 4-morpholineethanesulfonic acid; BCECF-AM, 3',6'-bis(acetyloxy)-5(or 6)-[[[acetyloxy)methoxy]carbonyl]-3-oxo-spiro[isobenzofuran-1(3H),9'-[9H]xanthene]-2',7'-dipropanoic acid 2',7'-bis[[[acetyloxy)methyl] ester].

mNect.hCNT3 H⁺/Uridine Co-transport

measure the current induced by addition of substrate in real-time, but they are time-consuming and require specialized equipment and skills. Radioisotope flux assays measure the accumulation of radiolabeled substrate. The need for radiolabeled substrate restricts the range of permeants able to be studied. In addition, radioisotope flux assays are not done in real-time and are labor-intensive, requiring large numbers of oocytes.

An attractive alternative approach for the study of hCNT3 would be to measure pH in the immediate vicinity of its intracellular face during H⁺/nucleoside co-transport. These measurements could take advantage of the remarkable progress achieved in the development of genetically encoded fluorophores (13). Indeed, all members of the extended family of homologues and variants of the *Aequorea victoria* green fluorescent protein (avGFP) exhibit pH-dependent changes in their fluorescent intensity. The spectral changes that occur upon a change in pH can be intensimetric (14), excitation ratiometric (14), emission ratiometric (15), or both excitation and emission ratiometric (16). The apparent pK_a (pK_a', equal to the pH at which the fluorescence is half-maximal in intensity) for a specific fluorescent protein (FP) is acutely dependent on specific amino acid substitutions in close proximity to the chromophore and can range from less than 3 (17, 18) to greater than 8 (19). Variants with pK_a' values that are relatively close to intracellular pH values (*i.e.* ~7.3 for the mammalian cytosol (20)) are particularly useful as genetically encoded biosensors for dynamic measurement of proton concentrations in living cells.

A major development in the area of FP technology has been the identification (21) and subsequent optimization (22, 23) of red fluorescent protein (RFP) homologues of avGFP. The first (monomeric RFP 1 (mRFP1)) (23) and second (the mFruit series) (22) generation-optimized RFPs, derived from tetrameric *Discosoma* RFP (21), suffer from relatively low brightness relative to other common hues of FP. For example, of the three most red-shifted second generation mFruit variants (mTangerine, mStrawberry, and mCherry) (22), the brightest (mStrawberry) has only 44% of the intrinsic brightness (proportional to the product of extinction coefficient (ϵ) and quantum yield (Φ)) of the popular yellow FP (YFP) Citrine (24) and 76% of the brightness of enhanced avGFP. This limitation has been partially addressed by third generation mRFPs, specifically mApple and TagRFP-T, with fluorescent brightness values on par with, or better than, that of enhanced avGFP (25).

Generally speaking, the most red-shifted RFPs derived from *Discosoma* RFP are relatively pH-insensitive, with the majority of variants having pK_a' values < 5 (22, 25). A notable exception is the recently reported mApple variant with a pK_a' of 6.5 (25). The more blue-shifted of the mFruit variants (*i.e.* mOrange) also have pK_a' values of 6.5 (22). Several variants of mRFP1 with pK_a' values >7.5 have been previously reported (26).

Here we report the engineering of a pH-sensitive mFruit variant through multiple rounds of directed evolution by random mutagenesis. This RFP, called mNectarine, is appropriate to measure physiological pH changes in mammalian cells, because it has a pK_a' of 6.9. We have developed a new method to measure H⁺/nucleoside co-transport in mammalian cells, which uti-

lizes hCNT3's H⁺ coupling characteristics and the pH sensitivity of mNectarine. We fused mNectarine to the cytosolic N terminus of hCNT3 to generate mNect.hCNT3. Fusion of the fluorescent H⁺ sensor to hCNT3 enabled measurement of pH at the intracellular surface of hCNT3, and provided insight into the mechanism of hCNT3 H⁺/uridine co-transport.

EXPERIMENTAL PROCEDURES

Materials—Synthetic DNA oligonucleotides for cloning and library construction were purchased from Integrated DNA Technologies (Coralville, IA). PCR products and products of restriction digests were purified by agarose gel electrophoresis and extraction using the GenCatch™ gel extraction kit (Epoch Biolabs, Sugar Land, TX) or QIAquick® Gel Extraction kit (Qiagen, Mississauga, Ontario, Canada). Plasmid DNA was purified from bacterial cultures, using the GeneJET™ Plasmid Miniprep kit (Fermentas, Ontario, Canada) or the HiSpeed® Plasmid Purification kit (Qiagen). Restriction endonucleases were purchased from either Invitrogen or New England Biolabs (Ontario, Canada). PNGaseF and T4 DNA ligase were from New England Biolabs. Dye terminator cycle sequencing reactions were performed using the DYEnamic ET kit (Amersham Biosciences) and were analyzed at the University of Alberta Molecular Biology Service Unit. ECL chemiluminescent reagent was from PerkinElmer Life Sciences. Ammonium persulfate was from Bioshop Canada Inc. (Burlington, Ontario, Canada). Acrylamide was from Bio-Rad. Protease inhibitor mixture tablets were from Roche Applied Sciences. Donkey anti-rabbit IgG conjugated to horseradish peroxidase (SC-2317) was from Santa Cruz Biotechnology, Inc. (Santa Cruz, CA). Anti-RFP rabbit polyclonal antibody (ab34771) was from abcam (Cambridge, MA). Poly-L-lysine, nigericin sodium salt, uridine, 3', 6'-bis(acetyloxy)-5(or 6)-[[acetyloxy)methoxy]carbonyl]-3-oxo-spiro[isobenzofuran-1(3H),9'-[9H]xanthene]-2',7'-dipropanoic acid 2',7'-bis[(acetyloxy)methyl] ester (BCECF-AM) and 5-(*N*-ethyl-*N*-isopropyl)amiloride (EIPA) were from Sigma-Aldrich Canada (Oakville, Canada). Platinum® Pfx DNA polymerase, Dulbecco's modified Eagle medium, calf serum, fetal bovine serum, and penicillin-streptomycin-glutamine were from Invitrogen. Round coverslips and *N,N,N',N'*-tetramethylethylenediamine were from Fisher Scientific. Excitation and emission filters for fluorescence screening and photometry were purchased from Chroma Technology (Rockingham, VT). The nucleotide sequence of mNectarine has been deposited in the GenBank™ nucleotide sequence data base under accession number FJ439505.

Mutagenesis, Library Construction, and Screening—Mutagenesis of cDNA was performed by overlap extension PCR (23) or error-prone PCR (24). PCR products were digested with XhoI and EcoRI and ligated into pBAD/His B vector digested with the same two enzymes, and used to transform electrocompetent *Escherichia coli* strain DH10B (Invitrogen), which were then plated on agar plates, containing LB-AMP (Luria-Bertani medium supplemented with 0.1 mg/ml ampicillin and 0.02% w/v L-arabinose). Plates were incubated for 14 h at 37 °C prior to library screening. Our previously described imaging system (27), was equipped with a 520–550 nm bandpass filter for excitation of red fluorescence from bacterial colonies plated on a

10-cm Petri dish. The fluorescence emission of individual colonies was screened by eye, using tinted plastic goggles that block light with a wavelength of less than 600 nm. In each round of screening, ~10⁵ colonies were visually inspected, and those with the most intense fluorescence (~10–20) were picked for further investigation. Colonies of interest were cultured overnight in 4 ml of LB-AMP. The following day 0.1 ml of each culture was dispensed into individual wells of a clear bottom 96-well plate (Nunc, Rochester, NY), and the full emission spectra of each variant measured with a Safire2 plate reader equipped with monochromators (Tecan, Mannedorf, Switzerland). Variants with the most intense red fluorescence emission were used as templates in the subsequent round of library construction. The resultant clone was called mNectarine in pBAD/His B.

Construction of Fusion Proteins—Mammalian expression construct mNectarine (pDEJ6) was generated by digestion of mNectarine in pBAD/His B with XhoI and EcoRI and ligation into pcDNA3.1(–) (Invitrogen). hCNT3 in the mammalian expression vector pcDNA3.1(+) was generated by digestion of hCNT3 in yeast expression vector pYPGE15 (28) with KpnI and EcoRI and ligation into pcDNA3.1(+) (Invitrogen). mNectarine.hCNT3 (pDEJ13) was constructed by two steps of PCR and cloning. The forward primer (5′-GCGGTACCGGTGGT-GAGCTGAGGAGTACAGCAGC-3′) included a KpnI site, two glycine codons, and the first 20 bp of hCNT3. The reverse primer (5′-GCCTCGAGTCAAATGTATTAGAGAT-3′) included an XhoI site and the last 18 bp of hCNT3. The cDNA was generated by PCR (30 cycles of 94 °C for 30 s, 50–63 °C for 60 s, and 72 °C for 120 s) and inserted into the KpnI and XhoI sites of the mammalian expression vector pcDNA3.1(+) to generate pDEJ11. The forward primer (5′-GCGCCAAGCT-TATGGTGAGCAAGGGCGAGG-3′) included a HindIII site plus the first 19 bp of mNectarine. The reverse primer (5′-GCGGTACCCTTGACAGCTCGTCCATGCC-3′) deleted the stop codon of mNectarine, included a KpnI site, and the last 21 bp of mNectarine. The cDNA was generated by PCR (30 cycles of 94 °C for 30 s, 63 °C for 60 s, and 72 °C for 120 s) and was inserted into the HindIII and KpnI sites of pDEJ11 to generate pDEJ13. mNectarine.hCNT3-F563C (pDEJ20) was constructed by digestion of pDEJ13 and hCNT3-F563C in oocyte expression vector pGEMHE (described previously) (29) by digestion with BamHI and EcoRV, and ligation. This introduced the F563C mutation into mNect.hCNT3. All fusion protein sequences were confirmed by sequencing (DNA Core Services Laboratory, Dept. of Biochemistry, University of Alberta).

Protein Purification and Characterization—For production of mNectarine protein, *E. coli* strain LMG194 was transformed with the pBAD/His B expression vector containing the FP gene of interest. A single colony was used to inoculate a 4-ml culture that was allowed to grow overnight (37 °C, 225 rpm) before being diluted into 1 liter of LB-AMP. The culture was grown for 12 h before cells were harvested by centrifugation and lysed by French Press. Proteins were purified by nickel-nitrilotriacetic acid chromatography (Amersham Biosciences), and then dialyzed into 5 mM Tris buffer, pH 7.5. Absorption spectra were recorded on a DU-800 UV-visible spectrophotometer (Beckman Coulter, Mississauga, Ontario, Canada), and fluorescence

excitation and emission spectra were recorded on a Safire2 plate reader. Fluorescence pK_a' measurements were performed by diluting the dialyzed protein into a series of buffered solutions (200 mM imidazole, 200 mM citric acid, and 200 mM sodium phosphate), previously adjusted to various pHs. Quantum yields were determined using mTangerine as the reference standard (22). Protein concentrations used for calculation of extinction coefficients were determined by the BCA method (Pierce).

Photostability Measurements—For photostability measurements, microdroplets were formed by vortexing a solution of the purified protein (100 μM protein in 5 mM Tris buffer, pH 7.5) mixed with mineral oil (17, 30). A sample of this suspension (~50 μl) was sandwiched between a glass slide and a glass coverslip. The slide was imaged on an Axiovert 200M inverted fluorescence microscope (Zeiss) equipped with a 75-watt xenon-arc lamp, a 20× objective, a 510–560 nm excitation filter, a 565 nm beamsplitter, a 573–648 nm emission filter, and a Retiga 2000R 12-bit cooled charge-coupled device camera (QImaging). Individual drops of protein solution considerably smaller than the field of view were identified by eye under low excitation light levels (2.5% neutral density filters). Digital image acquisition was then initiated, and the neutral density filters were removed. Collected images were processed using Image Pro (Media Cybernetics) to extract the fluorescence intensity as a function of time. Photobleaching curves were processed such that the bleaching half-time represents the time to bleach from an emission rate of 1000 photons/molecule/s to 500 photons/molecule/s (30). mTangerine was subjected to bleaching under identical conditions and used as a reference standard (22).

Tissue Culture—mNectarine, mNectarine.hCNT3, mNectarine.hCNT3-F563C, and hCNT3 constructs were expressed by transient transfection of HEK293 cells (31), using the calcium phosphate method (32). Cells were grown at 37 °C in an air/CO₂ (19:1) environment in Dulbecco's modified Eagle's medium (supplemented with 5% (v/v) fetal bovine serum, 5% (v/v) calf serum, and 1% (v/v) penicillin-streptomycin-glutamine). In experiments where fluorescence of intact HEK293 cells was monitored, HEK293 cells grown on poly-L-lysine-coated 25-mm round coverslips were transiently transfected with the appropriate cDNA.

PNGaseF Treatment and Immunodetection—HEK293 cells were transiently transfected with vector, mNectarine.hCNT3, or mNectarine.hCNT3-F563C cDNA. Cell lysates were harvested in IPB buffer (1% Nonidet P-40, 5 mM EDTA, 0.15 M NaCl, 0.5% deoxycholate, 10 mM Tris-HCl, pH 7.5). Samples (20 μg of protein) were combined with 2 μl of glycoprotein denaturing solution (0.5% SDS, 40 mM dithiothreitol) and water to make a 20-μl reaction volume. Samples were denatured by heating to 100 °C for 10 min. Reactions were made to 40 μl by addition of 4 μl of 10× G7 reaction buffer (50 mM sodium phosphate, pH 7.5), 4 μl of 10% Nonidet P-40, 1 μl of PNGaseF enzyme, and water. Samples were incubated at 37 °C for 1 h. One volume of 2× SDS-PAGE sample buffer (20% (v/v) glycerol, 2% (v/v) 2-mercaptoethanol, 4% (w/v) SDS, 1% (w/v) bromphenol blue, 150 mM Tris, 2× protease inhibitor mixture, pH 6.8) was added to each sample. Prior to analysis, samples

mNect.hCNT3 H⁺/Uridine Co-transport

were heated for 5 min at 65 °C and sheared through 21- and 26-gauge needles (BD Biosciences). Samples were resolved by SDS-PAGE on 7.5% acrylamide gels (33). Proteins were transferred to polyvinylidene difluoride membranes by electrophoresis for 1 h at 100 V at 20 °C in 10% (v/v) methanol, 25 mM Tris, and 192 mM glycine (34). Polyvinylidene difluoride membranes were blocked by incubation for 1 h at 20 °C in TBST-M buffer (TBST buffer (0.1% (v/v) Tween 20, 137 mM NaCl, 20 mM Tris, pH 7.5), containing 10% (w/v) nonfat dry milk) and then incubated at 4 °C for 16–18 h in TBST-M containing 1:10,000 diluted rabbit anti-RFP polyclonal antibody. Blots were incubated for 1 h with TBST-M containing 1:5000 diluted donkey anti-rabbit IgG conjugated to horseradish peroxidase. Blots were visualized using ECL reagent and a Kodak Image Station 440CF.

Measurement of Fluorescence in Intact HEK293 Cells—HEK293 cells, grown, and transfected on 25-mm glass coverslips were mounted in a 35-mm diameter Attofluor Cell Chamber (Molecular Probes). The chamber holds a custom-built insert, reducing the internal diameter to 13 mm and chamber volume to 0.2 ml. The chamber was placed on a Leica DMIRB inverted microscope, equipped with a Photon Technologies International (PTI) D-104 microscope photometer. The light source, connected to the microscope via a fiber optic cable, was a 75-watt xenon arc lamp in a PTI DeltaScan excitation monochromator, equipped with a chopper to enable dual excitation wavelength measurements. Excitation wavelengths were set to 550 nm (when monitoring mNect), or 440 and 502.5 nm (when monitoring BCECF). Wavelengths of emitted light were selected with a cube mounted in the microscope, containing either a 570 nm beamsplitter and a 575–625 nm emission filter (mNect) or a 515 nm beamsplitter and a 522.5–547.5 nm emission filter (BCECF).

Spectral Characterization of mNectarine Expressed in HEK293 Cells—HEK293 cells, transiently transfected with mNect cDNA, were solubilized with 5% Triton X-100, 50 mM phosphate, pH 7.6, and lysates collected following centrifugation for 2 min at 18,300 × *g*. Lysate was added to 50 mM phosphate, pH 7.6, and excitation and emission scans were collected at respective fixed emission and excitation wavelengths 590 and 550 nm, with sample in the cuvette of a PTI fluorometer. Scans were normalized by setting peak fluorescence to 1.0.

To measure spectral characteristics of intact HEK293 cells, cells were mounted on the microscope stage, as described above, and cytosolic pH was clamped to be the same as extracellular pH by perfusion in pH clamping buffer (5 mM glucose, 140 mM KCl, 5 mM potassium gluconate, 1 mM calcium gluconate, 1 mM MgSO₄, 2.5 mM sodium phosphate, 30 mM Hepes), containing 20 μM nigericin, with pH set to 6.5, 7.0, and 7.5. The photometer and microscope were configured for mNect fluorescence measurements, as described above. Excitation scans from 505–565 nm were collected, and all data (mNect and vector alone transfected cells) were normalized to the peak fluorescence value found for mNect-transfected cells clamped to pH 7.5.

Calibration of Fluorescence Values for pH—To convert the fluorescence values observed with pH reporters, BCECF, and mNect, transfected-HEK293 cells mounted on the microscope

stage were sequentially perfused with pH clamping buffers at pH values of ~6.5, 7.0, and 7.5 (35). Fluorescence counts for BCECF or mNect were measured, and in the case of mNect fluorescence, data were corrected for photobleaching (see below). A calibration curve relating the average fluorescence at each pH to the medium pH value was fitted to a straight line by linear regression. The resulting equation for the line was used to transform fluorescence count data to intracellular pH.

H⁺/Uridine Co-transport Activity Assay—Transfected HEK293 cells mounted on the microscope stage, as described above, were perfused at 3.5 ml/min consecutively with Na⁺-free MBSS buffer (90 mM choline chloride (ChCl), 5.4 mM KCl, 0.4 mM MgCl₂, 0.4 mM MgSO₄, 5.5 mM glucose, 100 mM D-mannitol, 10 mM MES, pH 7.5), Na⁺-free MBSS buffer, pH 5.5, and Na⁺-free MBSS buffer, pH 5.5, with 0.5 μM uridine. Alternatively, cells were perfused consecutively with Na⁺-free MBSS buffer, pH 5.5, Na⁺-containing MBSS buffer (90 mM NaCl, 5.4 mM KCl, 0.4 mM MgCl₂, 0.4 mM MgSO₄, 5.5 mM glucose, 100 mM D-mannitol, 10 mM MES), pH 5.5, and Na⁺-containing MBSS buffer, pH 5.5, with 0.5 μM uridine. Some experiments contained 0.5 μM EIPA. At the end of each experiment, cells were subjected to pH calibration, using the nigericin/high potassium method (described above). Rates of pH_i change during the 20-s periods before and after addition of uridine were determined as the slope (dpH_i/dt) of the line fitted by the least squares method. Uridine-induced pH_i change was calculated as: dpH_i/dt after addition of uridine minus dpH_i/dt before uridine addition. H⁺ Flux, in units of dpH_i/dt , was converted to flux of proton equivalents/time by multiplying dpH_i/dt by the previously established intrinsic buffer capacity of HEK293 cells (36). These experiments were performed in nominally CO₂/HCO₃⁻-free conditions, so it was assumed that the CO₂ buffer capacity would be negligible.

Photobleaching Correction—Cells were excited as described above, and fluorescence values over time were converted to F/F_0 and fitted with an exponential decay equation of the form,

$$Y = \text{span} \cdot \exp(-K \cdot X) + \text{plateau} \quad (\text{Eq. 1})$$

where fluorescence starts at Span + Plateau and decays to plateau with rate constant K. The half-life is 0.69/K. The variables over five experiments were averaged, and the data for each subsequent experiment was multiplied by the average decay equation.

Kinetics of H⁺/Uridine Co-transport—Experiments were carried out as described under H⁺/uridine co-transport activity assay with various concentrations of uridine (0–960 μM). Transport rates were obtained as described above, and plotted in Prism 4.0. Data were fitted with an equation of the form,

$$V = V_{\text{max}} \cdot [S] / (K_m + [S]) \quad (\text{Eq. 2})$$

where V_{max} is the velocity (V) at maximal substrate concentration ($[S]$) and K_m is the substrate concentration at which the rate is half-maximal.

Statistical Analysis—Values are expressed ± S.E. Statistical significance was determined using an unpaired *t* test (Prism), with $p < 0.05$ considered significant.

TABLE 1

Properties of mNectarine and related variants

Brightness is the product of extinction coefficient and quantum yield. For comparison, the brightness values of EGFP and mCherry are 34 and 16 $\text{mM}^{-1}\text{cm}^{-1}$, respectively (30). Photobleaching half-time represents the time to bleach from an initial emission rate of 1000 photons/molecule/s to 500 photons/molecule/s.

	Excitation maximum	Emission maximum	Extinction coefficient	Fluorescence quantum yield	Brightness	pK_a'	$t_{0.5}$ for maturation at 37 °C	$t_{0.5}$ for bleach (arc lamp)
	nm	nm	$\text{mM}^{-1}\text{cm}^{-1}$					s
mTangerine	568	585	38	0.30	11	5.7	1.5 h	5.1
mCherry2-M66C/Q213L	558	580	44 ^a	0.40 ^a	18	ND ^b	ND	ND
mNectarine	558	578	58 ^a	0.45 ^a	26	6.9	30 min	11

^a Measured in phosphate-buffered saline (pH 8.0), using mTangerine as the reference.

^b ND, not determined.

RESULTS

Engineering mNectarine—With the goal of engineering an mRFP with improved brightness, we chose mTangerine (the Q66C/T147S/Q213L variant of mRFP1) (22) for further optimization by directed evolution. We selected mTangerine because: 1) it has the highest fluorescence quantum yield of the most red-shifted second generation mRFPs (22); 2) its absorbance profile makes it well suited as a potential fluorescence resonance energy transfer acceptor from a YFP donor; and 3) relatively little effort had been previously expended on its optimization (22). We first transferred the characteristic mTangerine mutations (M66C and Q213L) to an engineered homologue that had already been subjected to extensive directed evolution for brightness and folding efficiency (mCherry2, the K92N/K138C/K139R/S147T/N196D/T202L variant of mCherry)⁸ (supplemental Fig. S1). mCherry2-M66C/Q213L had a fluorescence hue similar to that of mTangerine, yet had intrinsic fluorescent brightness that was 1.1× that of mCherry and 1.5× that of mTangerine (Table 1). This variant was used as the template for the first of five iterative rounds of random mutagenesis and manual fluorescence-based screening of large randomized libraries (each on the order of 10⁵ variants) expressed in bacterial colonies. In each round the brightest colonies were picked, plasmids isolated, and the pool of improved FP genes used as the template for the subsequent library. We have successfully applied this basic strategy to the optimization of a teal FP (27), blue FPs (17), and a YFP with violet excitation (37).

During this process, the protein accumulated four additional substitutions relative to the initial template: F91L, M141V, Y151H, and K162M. The resulting protein was an mRFP with intrinsic brightness (Table 1) that was considerably greater than that of mCherry and mTangerine (22) (1.6× and 2.3×, respectively) but still somewhat less than that of mApple and TagRFP-T (25) (0.71× and 0.78×, respectively). The excitation and emission maxima of the final variant (excitation maximum at 558 nm and emission maximum at 578 nm) were different enough from that of mTangerine, and every other variant in the existing palette, that we decided to designate it with the name “mNectarine” (supplemental Fig. S1).

pH Sensitivity of mNectarine—Characterization of mNectarine revealed that its fluorescence was remarkably pH-sensitive, with an apparent pK_a' of 6.9 (Fig. 1, A and B). The data points shown in Fig. 1B were fitted to a curve of the general form,

$$I_{\text{pH}} = \frac{I_{\text{max}}}{10^{(\text{pK}_a' - \text{pH})} + 1} \quad (\text{Eq. 3})$$

⁸ N. C. Shaner and R. Y. Tsien, unpublished results.

where I_{pH} is the fluorescence intensity at a given pH, and I_{max} is the highest fluorescence intensity at any pH. An equation of similar form was used to fit the absorbance data points as shown in Fig. 1D.

Absorbance spectra of mNectarine recorded at various pHs revealed a complex change in profile that appears to include a mixture of anionic cyan-absorbing ($\lambda_{\text{max}} = 489$ nm) and orange-absorbing ($\lambda_{\text{max}} = 558$ nm) forms of the protein at high pH and a mixture of protonated violet-absorbing ($\lambda_{\text{max}} = 387$ nm) and blue-absorbing ($\lambda_{\text{max}} = 453$ nm) forms of the protein at low pH (Fig. 1C). A reasonable explanation of these changes is that the purified and aged protein exists as a mixture of an orange-absorbing/red-fluorescing species and a “dead-end” cyan-absorbing/non-fluorescent species with an avGFP-type chromophore. Accordingly, the cyan and violet species may represent two ionization states of one distinct form of an avGFP-type chromophore, whereas the orange and blue species represent two ionization states of a *Discosoma* RFP-type (or possibly an mOrange-type, containing a third heterocycle (38)) chromophore. To investigate this hypothesis, we performed a multiple linear regression analysis of the spectra acquired at each pH to examine the relative contribution of each of these four components. Efforts to fit the data with fewer than four components resulted in poor fits of the experimental data. This analysis revealed that pH-dependent changes in the absorbance of the violet (decreasing with increasing pH) and cyan species (increasing with increasing pH) occur with pK_a' values of ~8.1 (Fig. 1D), an observation consistent with the conclusion that these are indeed different ionization states of the same molecular species. The multiple regression analysis did not provide support for correlated changes in the orange and blue species as a function of pH, with the intensity of blue species remaining relatively constant as the intensity of orange species changed considerably. Two possible explanations for this discrepancy are that either the blue peak represents a distinct dead-end species, or that our data are simply insufficient to enable separation of the overlapping contributions of the violet and blue peaks.

mNectarine.hCNT3 Fusion Proteins—We fused mNectarine to the N terminus of the human nucleoside transporter, hCNT3. The N terminus was chosen for the fusion, because the C terminus is extracellular (8), and our goal was to measure pH at the intracellular surface of hCNT3. We wanted to use a specific and localized probe of $[\text{H}^+]$ because hCNT3 has a relatively low turnover rate (a value of 34 s^{-1} for hCNT3 was found in voltage-clamped oocytes at -150 mV (39)). Because the rest-

mNect.hCNT3 H⁺/Uridine Co-transport

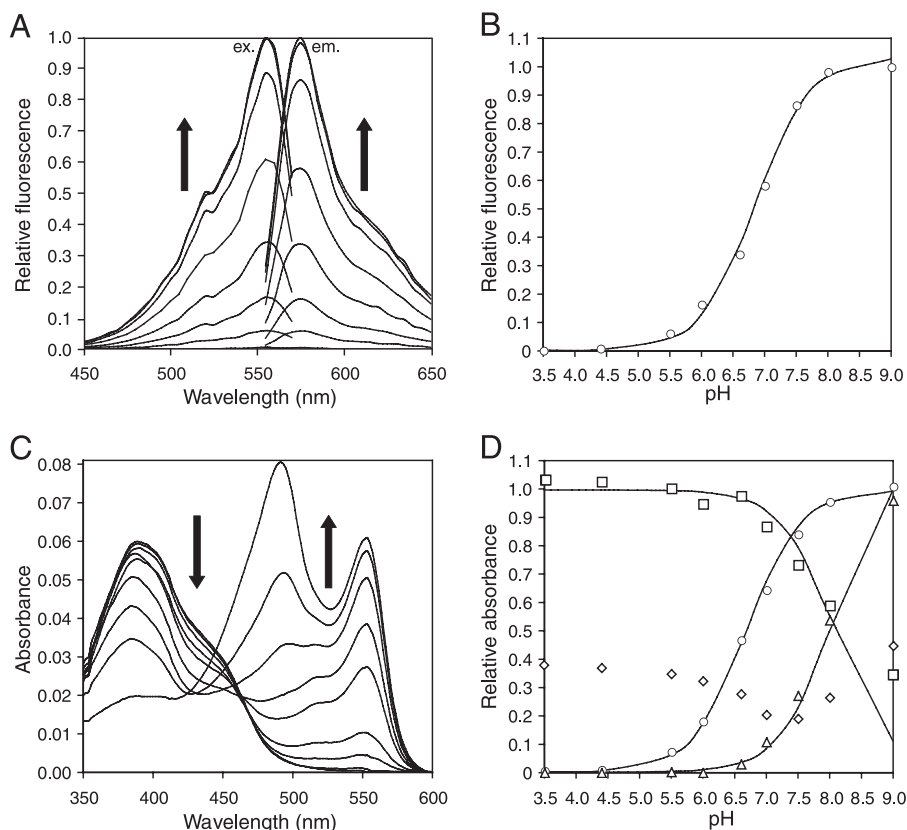


FIGURE 1. pH dependence of mNectarine fluorescence. *A*, fluorescence excitation (left, emission at 600 nm) and emission (right, excitation at 550 nm) intensity for mNectarine, recorded at various pH (actual pH values presented in *B*). Arrows represent the direction of change with increasing pH. *B*, plot of relative fluorescence intensity versus pH for mNectarine, with excitation at 550 nm and emission at 600 nm. The curve represents the best of fit of the data obtained using a form of the Henderson-Hasselbalch equation. *C*, absorbance spectra of mNectarine at various pH. Arrows represent the direction of change with increasing pH. These spectra were subjected to a global four-component linear regression analysis (supplemental Fig. S2). *D*, relative absorbance intensities of each component of the spectra in *C* plotted as a function of pH. The four components are the red fluorescence excitation profile (Δ , orange-absorbing) and three Gaussian curves centered at 489 nm (\square , cyan-absorbing), 453 nm (\diamond , blue-absorbing), and 387 nm (\square , violet-absorbing).

transiently transfected with vector, mNect.hCNT3, or mNect.hCNT3-F563C cDNA. Lysates from the cells were treated with or without PNGaseF (an enzyme that removes N-linked glycosylation from proteins (40)). Samples were immunoblotted and probed with an anti-RFP antibody. hCNT3 alone migrated as a 75 kDa band (12), whereas mNectarine was 27 kDa. Untreated mNect.hCNT3 was detected as multiple bands around 100 kDa (Fig. 2). Upon treatment with PNGaseF, only a single band was detected for the two fusion proteins (Fig. 2). The multiple banding pattern is attributed to unglycosylated, core glycosylated, and mature glycosylated bands. This is supported by the prediction that there are four putative glycosylation sites in the C terminus of hCNT3, and both hCNT1 and hCNT3 exhibit multiple glycosylation states (12, 41, 42). The presence of different glycoforms of hCNT3 will not affect the function of the protein at the plasma membrane, because hCNT3 with all glycosylation sites absent is fully functional (12).

Spectral Characterization of mNectarine Expressed in HEK293 Cells—Fluorescence excitation and emission scans were obtained for

lysates of mNect-transfected HEK293 cells (Fig. 3A). The peak fluorescence excitation wavelength was 558 nm, and the peak emission wavelength was 573 nm. Fluorescence excitation spectra were collected for intact mNect-transfected HEK293 cells, or vector-alone transfected cells clamped at pH 7.5, 7.0, and 6.5 with nigericin/high potassium (Fig. 3B). mNectarine fluorescence decreased with decreasing pH (Fig. 3B), in a manner similar to that seen with purified mNectarine (Fig. 1A). In intact HEK293 cells the peak excitation wavelength was 558 nm at pH 6.5 and 7.0, and 557 nm at pH 7.5 (Fig. 3B). The observed fluorescence of mNect-transfected cells can be attributed to mNect fluorescence, because little fluorescence was observed when similar numbers of vector-alone transfected HEK293 cells were subjected to fluorescence excitation scans (Fig. 3B, lower curves). A plot of normalized fluorescence in intact mNect-transfected cells versus medium pH revealed a linear relationship over the pH 6.5–7.5 range (Fig. 3C). This indicates that mNect fluorescence, upon appropriate calibration, can be used as a reporter of cytosolic pH in intact cells.

Correction for mNectarine Photobleaching—Extended periods of illumination of mNect, under pH-clamped conditions, resulted in a continuous decrease of fluorescence, consistent with photobleaching (Fig. 4A). Examination of the kinetics of

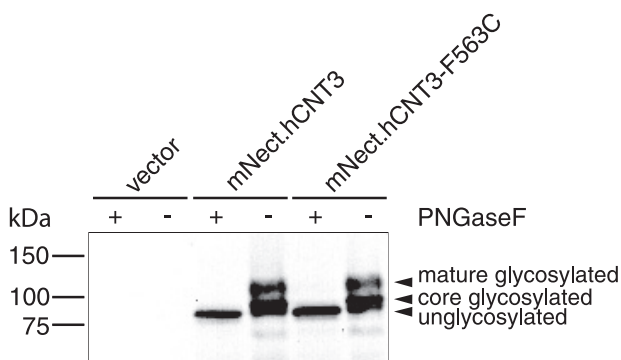


FIGURE 2. Expression of mNect.hCNT3 in HEK293 cells and analysis of glycosylation status. HEK293 cells were transiently transfected with vector (pcDNA3.1), mNectarine.hCNT3, or mNectarine.hCNT3-F563C cDNA. Lysates from the cells were treated with (+) or without (–) the deglycosylation enzyme, PNGaseF. Samples were immunoblotted and probed with a polyclonal anti-RFP antibody.

ing membrane potential of mammalian cells is ~ -40 mV, a turnover rate closer to 10 s^{-1} is to be expected.

Expression of mNect.hCNT3 fusion proteins was assessed on immunoblots (Fig. 2). hCNT3-F563C, a functionally inactive mutant (29), was fused to mNectarine to serve as a negative control (called mNect.hCNT3-F563C). HEK293 cells were

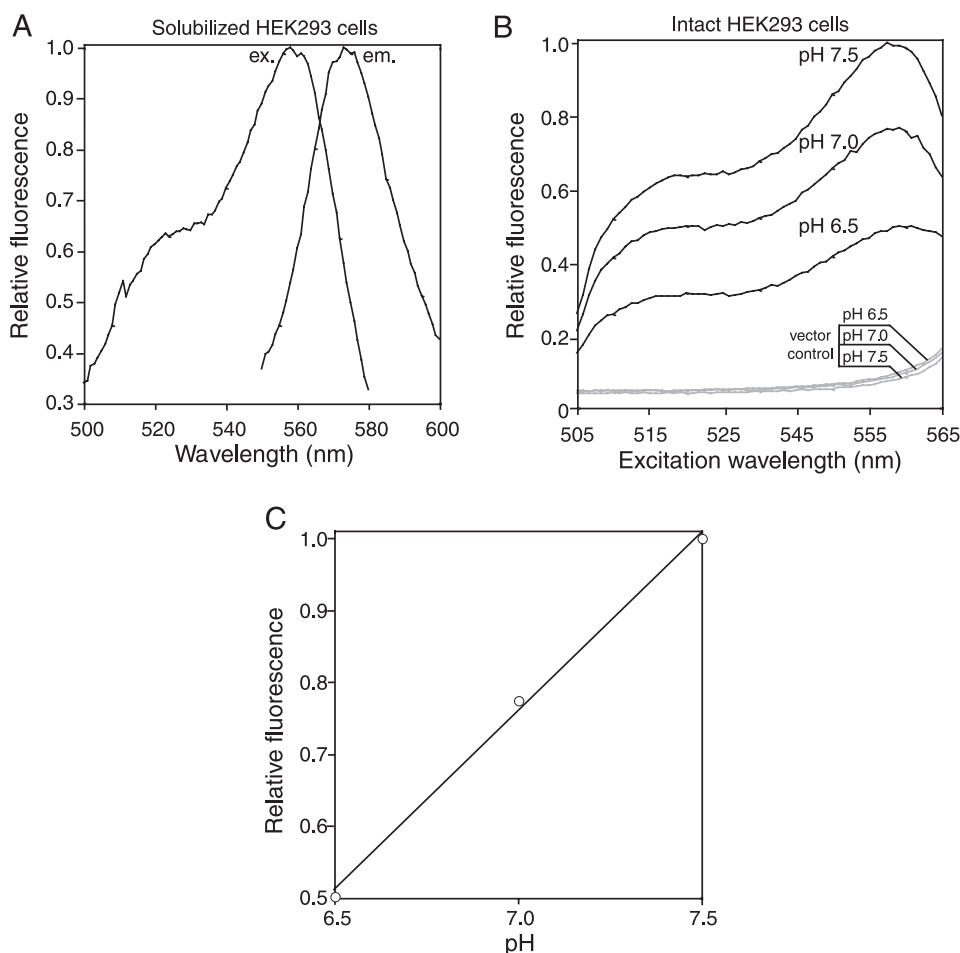


FIGURE 3. Spectral characterization of mNectarine expressed in HEK293 cells. HEK293 cells were transfected with mNectarine cDNA, and cell lysates were prepared. *A*, excitation (*ex.*) and emission (*em.*) scans of the lysates were collected at respective fixed emission and excitation wavelengths 590 and 550 nm. *B*, fluorescence excitation spectra ($\lambda_{em} = 573$ nm) of intact mNect-transfected HEK293 cells clamped at pH 7.5, 7.0, and 6.5 with nigericin/high potassium (*black lines*). Excitation spectra of vector-alone-transfected cells are shown as *gray lines*, with clamped pH values of experiments indicated. *C*, relationship between fluorescence ($\lambda_{ex} = 558$ nm and $\lambda_{em} = 573$ nm) and clamped cytosolic pH, in mNect-transfected HEK293 cells (data from *B*).

bleaching revealed they could be fitted by an exponential decay equation, which provides the basis for a method to correct for photobleaching. Under pH-clamped conditions mNect should report a constant fluorescence value, in the absence of photobleaching. The ability to correct photobleaching, by applying an exponential correction, was applied to pH 7.0-clamped cells (Fig. 4, *A* and *B*). The data revealed that the continuous reduction in signal was substantially corrected, but not fully eliminated. To limit the effects of photobleaching and the need to apply corrections, in further experiments, steps were taken to minimize the time period during which mNect was illuminated.

The ability for mNect to report cytosolic pH accurately, following photobleaching correction, was assessed by clamping cytosolic pH to medium pH, using the nigericin/high potassium method (Fig. 4, *C* and *D*). In these experiments pH was clamped sequentially to values near 7.0, 6.5, 7.5, and 7.0 (reported in Fig. 4, *C* and *D*, in the *black bar*) by perfusion with media of known pH. To calibrate fluorescence to cytosolic pH, a standard curve was generated, relating average fluorescence to media pH at each of the last three solutions. The average pH value during perfusion with each solution was then calculated (reported

adjacent to each curve, Fig. 4, *C* and *D*). The initial pH 7.00 perfusion data were not used to produce the standard curve (*pH versus fluorescence*), so the ability of mNect to report pH during this perfusion reveals the reliability of mNect during a typical experiment. Without photobleaching correction there are significant differences between the pH reported by mNect and the medium pH (Fig. 4*C*). In particular, during the initial perfusion with pH 7.00 medium, the data fitted a pH value of 7.22 (Fig. 4*C*). By contrast, the photobleaching correction greatly improved the concordance between medium pH and pH reported by mNect. Indeed, mNect reported a pH of 6.97 during the initial pH 7.00 perfusion (Fig. 4*D*). Together these data reveal that after correction for photobleaching, mNect, calibrated by sequential perfusion with nigericin/high potassium media in the pH 6.5–7.5 range is able to report accurately on cytosolic pH.

Measurement of Cytosolic pH by mNect, mNect.hCNT3, and BCECF—To test the reliability of mNect and mNect.hCNT3 as reporters of cytosolic pH, we compared their ability to report cytosolic pH to data collected using the well established pH-sensitive dye, BCECF (Fig. 5). HEK293 cells were transiently co-transfected with cytosolic

mNectarine and hCNT3 cDNA, or mNect.hCNT3, or with hCNT3 alone. These latter cells were loaded with BCECF, by incubation with BCECF-AM. Cells were perfused with nigericin/high potassium solutions at pH 7.5, 6.5, and 7.0. As described above, the average fluorescence values at each medium pH were then used to construct a standard curve, which was then applied to the fluorescence data, to transform it to intracellular pH (Fig. 5). Comparison, between the pH of perfusion medium to reported cytosolic pH determined from fluorescence, reveals that mNect, mNect.hCNT3, and BCECF are similar in their ability to report cytosolic pH. We then measured the absolute difference in pH between the medium pH and the pH reported by BCECF and mNect.hCNT3 to provide a quantitative comparison of the reliability of the two fluorescent pH reporters. For BCECF the mean absolute difference was 0.013 ± 0.003 pH units ($n = 12$) and for mNect.hCNT3 the mean absolute difference was 0.038 ± 0.005 pH units ($n = 24$). We conclude that BCECF reports on cytosolic pH more accurately than mNect.hCNT3, but that mNect.hCNT3 can be expected to report on cytosolic pH within 0.04 pH units of the “true” cytosolic pH over the pH 6.5–7.5 range.

mNect.hCNT3 H⁺/Uridine Co-transport

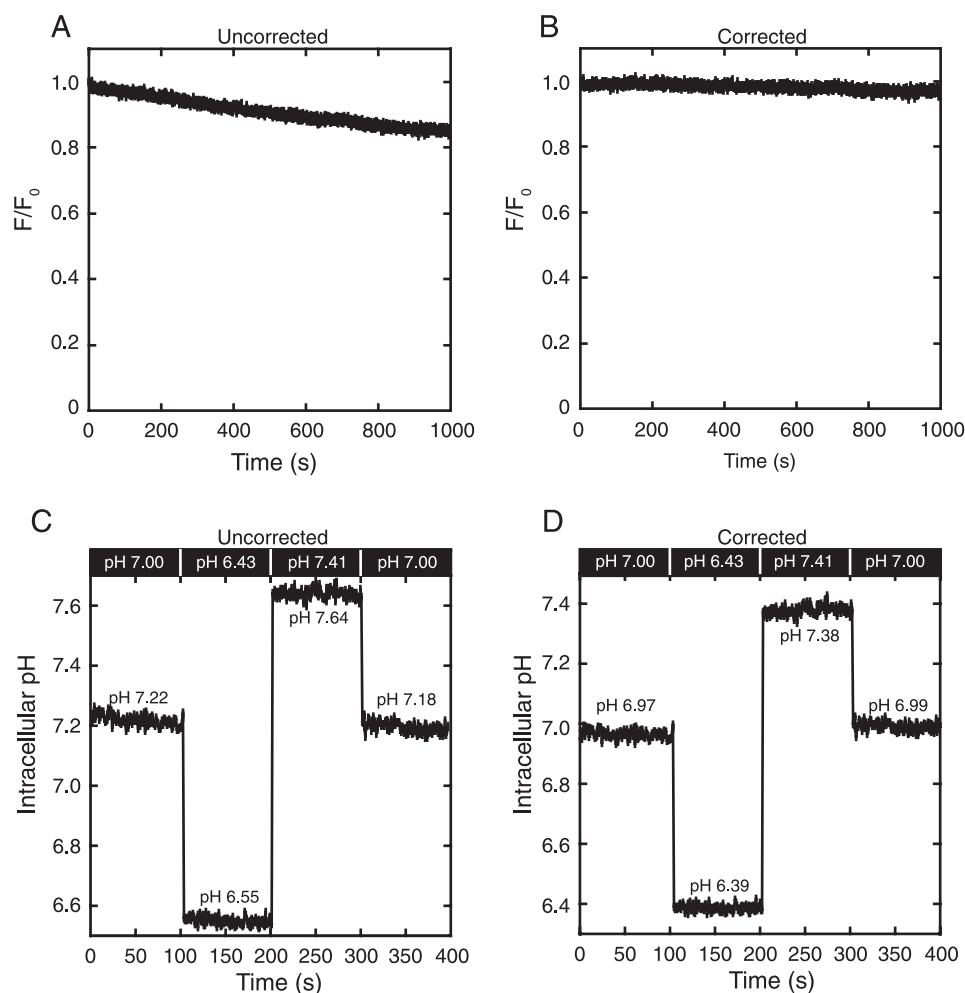


FIGURE 4. Correction for mNectarine photobleaching. HEK293 cells were transiently transfected with free cytosolic mNectarine cDNA, and fluorescence was monitored ($\lambda_{\text{ex}} = 550 \text{ nm}$ and $\lambda_{\text{em}} = 573 \text{ nm}$). *A* and *B*, cells were perfused with nigericin/high potassium solution, pH 7.0, to clamp intracellular pH. *A*, raw mNectarine fluorescence at pH 7.0, declining as a result of photobleaching. *B*, mNectarine fluorescence at pH 7.0. Data from *panel A* has been corrected for photobleaching, using the approach described in methods. *C* and *D*, HEK293 cells transfected with mNect cDNA were perfused consecutively with nigericin/high potassium solutions at pHs indicated in the black bars above the curves. To minimize the period of sample illumination, samples were perfused without illumination for 480 s in each solution prior to collecting fluorescence data. Above or below each trace are the average pH values for each perfusion interval, calculated from the fluorescence data. *C*, data not corrected for photobleaching. *D*, data from *panel C* corrected for photobleaching, using the approach described under "Experimental Procedures."

H⁺/Uridine Co-transport—We next examined the ability of the mNectarine.hCNT3 fusion proteins to report on changes in intracellular pH upon stimulation of H⁺/nucleoside co-transport. We used uridine as the nucleoside of choice because uridine elicits the largest nucleoside-induced inward currents under Na⁺-free, pH 5.5 conditions, which were previously found necessary for robust H⁺/uridine co-transport (10). HEK293 cells were transiently transfected with cDNAs encoding mNect.hCNT3 or mNect.hCNT3-F563C (Fig. 6). Cells were perfused consecutively with Na⁺-free MBSS buffer, in which ChCl was substituted for NaCl, at pH 7.5, Na⁺-free MBSS buffer, pH 5.5, and Na⁺-free MBSS buffer, pH 5.5, containing 0.5 mM uridine. Each experiment was then calibrated for pH using the nigericin/high potassium method (35). Co-transport of uridine with H⁺, which was initiated by the addition of uridine, was monitored by measuring intracellular pH (pH_i). Fluorescence data were corrected for photobleaching, and cor-

rected fluorescence data were converted to pH_i. Transport rates were determined by linear regression of the initial acidification rate from the first 20 s after addition of uridine minus the rate before addition of uridine.

pH 5.5 Na⁺-free MBSS medium induced a slow acidification of mNect.hCNT3 and mNect.hCNT3-F563C-transfected cells (Fig. 6, *A* and *B*), which is addressed below. The rate of acidification increased significantly upon addition of 0.5 mM uridine, only in mNect.hCNT3-expressing cells (Fig. 6, *A* and *B*), consistent with hCNT3-mediated H⁺-coupled uridine transport. Quantification of the change in the rate of acidification (proton flux in units of mM·min⁻¹) upon switching to uridine-containing medium revealed that cells transfected with mNect.hCNT3 had a proton flux of $1.08 \pm 0.10 \text{ mM}\cdot\text{min}^{-1}$, whereas cells transfected with the inactive hCNT3 mutant fusion protein, mNect.hCNT3-F563C, had a proton flux of $-0.02 \pm 0.1 \text{ mM}\cdot\text{min}^{-1}$ (Fig. 6*C*). Assuming a H⁺:nucleoside coupling stoichiometry of 1:1, as found for hCNT3 uridine transport when expressed in *Xenopus laevis* oocytes (9, 10), these data imply that the rate of change of cytosolic concentration of uridine is the same as the rate of change of [H⁺], found using mNect.hCNT3. Together these results demonstrate that the mNect.hCNT3 fusion protein reports on H⁺/uridine co-transport

by sensing changes in pH_i associated with coupled H⁺/uridine influx.

One caveat, however, relates to the calculation of proton flux, using the established buffer capacity of the bulk cytosol of HEK293 cells. We measured intracellular pH using mNect.hCNT3, anchored at the surface of the plasma membrane. If the buffer capacity at the membrane surface, in the vicinity of mNect.hCNT3, differs from bulk cytosol, it would affect the conversion of dpH/dt values to H⁺ flux. That said, the buffer capacity at the membrane surface is a constant; transport rates can therefore be reliably compared between different cell samples, as the buffer capacity would be the same between them. Further, it is unlikely that the buffer capacity at the plasma membrane surface differs dramatically from bulk cytosol.

Because point mutations can sometimes impair trafficking of membrane proteins, we assessed the plasma membrane localization of mNect.hCNT3 compared with mNect.hCNT3-

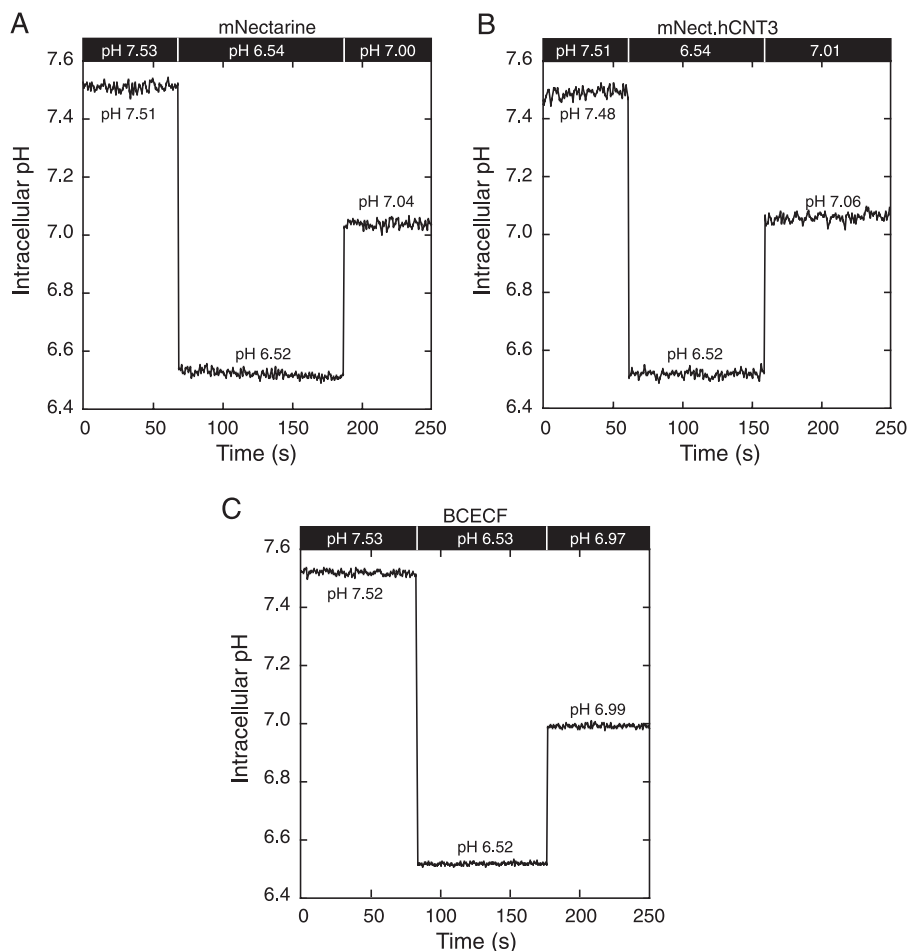


FIGURE 5. Measurement of intracellular pH, using cytosolic mNectarine, mNect.hCNT3, and BCECF. HEK293 cells were transiently co-transfected with cytosolic mNectarine and hCNT3 cDNA (A) or mNect.hCNT3 cDNA (B) or hCNT3 cDNA (C). hCNT3-transfected cells were incubated with the pH-sensitive dye BCECF-AM (C). Cells were perfused with nigericin/high potassium calibration solutions at pH values indicated in the black bars above the curves to calibrate fluorescence to pH. To minimize the period of sample illumination, samples were perfused without illumination for 480 s in each solution prior to collecting fluorescence data. Average pH values for each perfusion interval (calculated from the fluorescence data) are indicated above or below the trace. A and B, mNect fluorescence ($\lambda_{\text{ex}} = 550$ nm and $\lambda_{\text{em}} = 573$ nm) was corrected for photobleaching. C, BCECF fluorescence was monitored at $\lambda_{\text{ex}} = 440$ nm and 502.5 nm and $\lambda_{\text{em}} = 528.7$ nm.

F563C. HEK293 cells transfected with either mNect.hCNT3 or mNect.hCNT3-F563C cDNA had similar degrees of plasma membrane localization on the basis of imaging mNectarine fluorescence by confocal microscopy (data not shown).

To assess the reliability of the mNect.hCNT3 fusion as an assay for H⁺/nucleoside co-transport, we measured the K_m of mNect.hCNT3 for uridine. HEK293 cells were transiently transfected with mNect.hCNT3 cDNA, and were consecutively perfused with Na⁺-free MBSS buffer at pH 7.5, Na⁺-free MBSS buffer, pH 5.5, and Na⁺-free MBSS buffer, pH 5.5, containing varying amounts of uridine, from 0 to 960 μM . The change in the rate of acidification (proton flux in units of $\text{mM}\cdot\text{min}^{-1}$) was quantified upon switching to uridine-containing medium at each concentration of uridine. Fig. 7 shows a representative example of three separate experiments used to calculate the K_m for uridine transport in HEK293 cells, as measured with mNect.hCNT3. The K_m determined was 72 ± 24 μM ($n = 3$), which lies between the two previously published values of 110 ± 10 μM and 62.4 ± 5.4 μM found in oocytes (10, 12). We conclude that measurement of uridine flux by following H⁺

movement with mNect.hCNT3 is an accurate assay of H⁺/nucleoside co-transport.

Radiolabeled substrate uptake studies in oocytes found that uridine is transported to a similar extent in both acidic Na⁺-free and acidic Na⁺-containing conditions (10, 12). Charge/uptake experiments suggested that in Na⁺-containing buffer, pH 5.5, both Na⁺ and H⁺ contribute to the driving force, and that one of the two Na⁺ binding sites is shared by H⁺ (10). To determine whether a H⁺ is co-transported with uridine in acidic Na⁺-containing medium, HEK293 cells were transiently transfected with mNect.hCNT3 or mNect.hCNT3-F563C cDNA: Cells were perfused with Na⁺-free MBSS buffer, pH 5.5, in which NaCl was replaced by ChCl, Na⁺-containing MBSS buffer, pH 5.5, and Na⁺-containing MBSS buffer, pH 5.5, containing 0.5 mM uridine. The Na⁺/H⁺ exchange inhibitor, EIPA (5 μM), was present in all perfusion buffers. The data were collected and analyzed as described above.

Addition of uridine induced acidification in both Na⁺-free (Fig. 8B) and Na⁺-containing medium (Fig. 8A) in mNect.hCNT3-transfected cells. Cells expressing catalytically inactive mNect.hCNT3-F563C had no increase in acidification rate upon addition of uridine to the medium (Fig. 8C). Quantification of the increase in acidification rate following addition of uridine (Fig. 8D) revealed that Na⁺ had no effect on the acidification rate (1.09 ± 0.11 or 1.18 ± 0.32 $\text{mM}\cdot\text{min}^{-1}$, in the absence or presence of Na⁺, respectively). This provides support for the proposed mechanism that in acidic Na⁺-containing conditions, 1 Na⁺ and 1 H⁺ are transported per uridine molecule, while in acidic Na⁺-free conditions, 1 H⁺ alone is transported per uridine molecule (9–12).

Prior to the addition of uridine, the mNect.hCNT3-F563C transfected cells acidified to a lesser extent than the mNect.hCNT3-transfected cells (Fig. 6), but this difference was found to be not statistically significant (data not shown). We reasoned that Na⁺-free medium might cause the plasma membrane Na⁺/H⁺ exchanger (NHE) to act in reverse mode, exporting Na⁺ and importing H⁺, resulting in acidification upon switching from Na⁺-containing to Na⁺-free medium. Indeed, cytosolic acidification was found in Na⁺-free medium, but only at pH 5.5, not at pH 7.5 (Fig. 6, A and B). Because acidification rates were similar in cells expressing functional and catalytically

mNect.hCNT3 H⁺/Uridine Co-transport

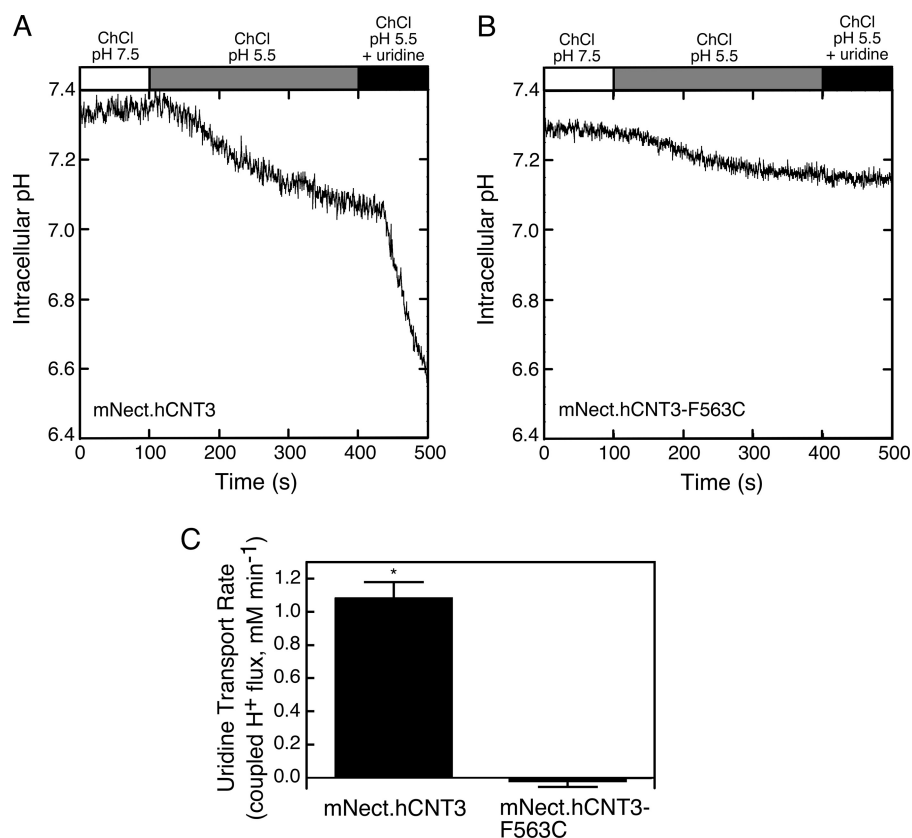


FIGURE 6. hCNT3 mediated H⁺/uridine co-transport measured by mNectarine-hCNT3. HEK293 cells were transiently transfected with mNect.hCNT3 cDNA (A) or with mNect.hCNT3-F563C cDNA (B). mNect.hCNT3 fluorescence was monitored at $\lambda_{\text{ex}} = 550$ nm and $\lambda_{\text{em}} = 573$ nm. Cells were perfused consecutively with Na⁺-free MBSS buffer, pH 7.5 (open bar), in which NaCl is replaced by choline chloride, Na⁺-free MBSS buffer, pH 5.5 (gray bar), and Na⁺-free MBSS buffer with 0.5 mM uridine, pH 5.5 (black bar). At the end of each experiment photobleaching-corrected fluorescence values were calibrated to pH via the nigericin/high potassium technique (not shown in figure) (35). A, pH, transients observed for mNectarine.hCNT3-transfected cells. B, pH, transients observed for mNect.hCNT3-F563C-transfected cells. C, quantification of the change in rate of acidification (proton flux in units of $\text{mM}\cdot\text{min}^{-1}$) upon switching to uridine-containing medium. Error bars represent standard error ($n = 5$). Asterisk indicates significant difference ($p < 0.0001$).

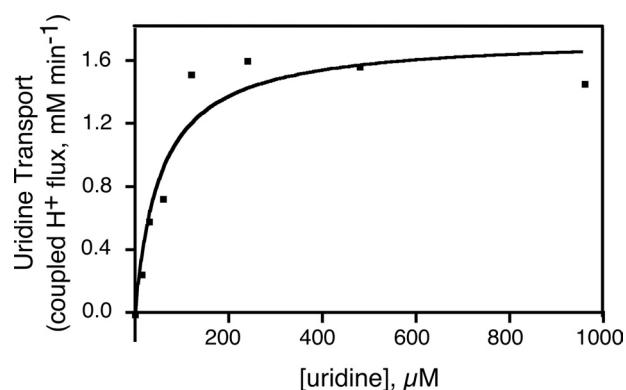


FIGURE 7. Kinetics of H⁺/uridine co-transport in HEK293 cells. HEK293 cells were transiently transfected with mNect.hCNT3 cDNA. mNect.hCNT3 fluorescence was monitored at $\lambda_{\text{ex}} = 550$ nm and $\lambda_{\text{em}} = 573$ nm. Cells were perfused consecutively with Na⁺-free MBSS buffer, pH 7.5, in which NaCl is replaced by choline chloride, Na⁺-free MBSS buffer, pH 5.5, and Na⁺-free MBSS buffer, pH 5.5, containing varying concentrations of uridine from 0 to 960 μM . At the end of each experiment pH was calibrated via the nigericin/high potassium technique, and fluorescence values were calibrated to pH. The change in the rate of acidification (proton flux in units of $\text{mM}\cdot\text{min}^{-1}$) was quantified upon switching to uridine-containing medium at each concentration of uridine. This graph is a representative example of three separate experiments used to calculate the K_m of mNect.hCNT3 for uridine.

inactive hCNT3 (Fig. 6, A and B), the acidification mechanism is inherent to the HEK293 cells. To assess the possible role of NHE in cytosolic acidification 5 μM EIPA, a Na⁺/H⁺ exchange inhibitor (43), was added to media (Fig. 8). EIPA was unable to suppress the acidification rate in Na⁺-free medium (Fig. 8B). Together these data suggest that there is an H⁺ leak into HEK293 cells in acidic Na⁺-free medium that is independent of NHE and hCNT3. The identity of the pathway is unknown, but H⁺ leak through cation channels has been reported (44, 45). The background H⁺ leak can be avoided by in mNect.hCNT3 assays of H⁺/uridine co-transport in the presence of Na⁺, because no acidification was found at pH 5.5 until uridine was added to mNect.hCNT3-expressing cells (Fig. 8, A and C).

DISCUSSION

We utilized hCNT3's H⁺-coupling characteristics to develop a new method to assay nucleoside transport in cultured mammalian cells. This assay was made possible by engineering a new pH-sensitive red fluorescent protein, mNectarine. mNectarine, fused to the N terminus of hCNT3, was able to reliably

report on changes in pH at the intracellular surface of hCNT3 in real-time. Addition of uridine to mNect.hCNT3-expressing cells, in both Na⁺-free and Na⁺-containing conditions elicited an increase in the rate of acidification that was not seen in the negative control (mNect.hCNT3-F563C-expressing cells). Our data are consistent with hCNT3-mediated Na⁺/H⁺/nucleoside co-transport under acid conditions.

Using mNect.hCNT3 to measure uridine flux by monitoring H⁺ co-transport is advantageous, because it enables direct measurement of changes in intracellular H⁺ concentration, which, up until now, had only been inferred from H⁺ activation of [¹⁴C]uridine influx and pH-dependent uridine-evoked currents in oocytes (8, 9, 29). The present experiments therefore provide the first direct evidence that hCNT3 transports H⁺. Because we did not directly measure uridine flux in these experiments, it is formally possible that the mNect.hCNT3 assay measures an hCNT3-mediated H⁺ flux unrelated to uridine transport. We consider this unlikely, because under similar extracellular acid medium conditions uptake of radioactive nucleoside was observed in oocytes (9, 10).

We assessed the reliability of mNect.hCNT3 as a reporter for hCNT3 H⁺/nucleoside co-transport, by measuring the K_m of mNect.hCNT3 for uridine. The K_m determined here (72 ± 24

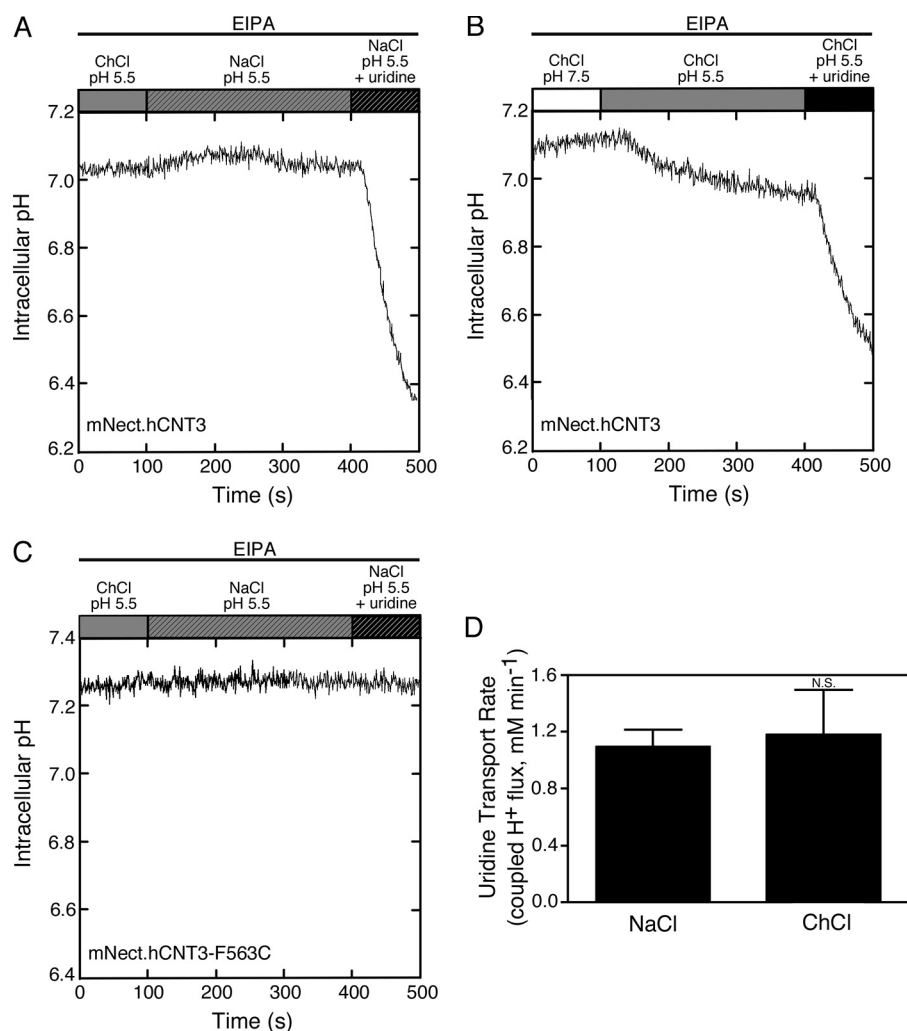


FIGURE 8. Effect of Na⁺ on H⁺/uridine co-transport. HEK293 cells were transiently transfected with mNectarine. hCNT3 cDNA (A and B) or with mNect.hCNT3-F563C cDNA (C). mNect.hCNT3 fluorescence was monitored at $\lambda_{\text{ex}} = 550$ nm and $\lambda_{\text{em}} = 573$ nm. Cells were perfused with MBSS buffer, pH 5.5 (gray bars), or MBSS buffer, pH 5.5, containing 0.5 mM uridine (black bars). Perfusion with Na⁺-containing MBSS buffer is indicated by hatched bars, and perfusion with Na⁺-free MBSS buffer, in which NaCl is replaced by choline chloride (ChCl), is indicated by un-hatched bars. Open bar indicates perfusion with Na⁺-free MBSS, pH 7.5. All buffers contained 5 μM EIPA. D, quantification of the change in rate of acidification (proton flux in units of $\text{mM}\cdot\text{min}^{-1}$) upon switching to uridine-containing medium. Error bars represent standard error ($n = 3$). N.S. indicates non-significant difference ($p = 0.81$).

μM) was between two previously published values for hCNT3 expressed in oocytes (110 ± 10 and $62 \pm 5 \mu\text{M}$) (10, 12), indicating that mNect.hCNT3 provides an accurate method to measure hCNT3 kinetics.

This study illuminates the mechanism of nucleoside transport under conditions of extracellular acid and Na⁺. Previous investigations in *X. laevis* oocytes demonstrated that uridine was transported with high efficiency in both Na⁺-containing medium at pH 5.5, and Na⁺-free medium at pH 5.5, although to a somewhat lesser extent under Na⁺-free conditions (10, 12). hCNT3 co-transport of nucleoside with Na⁺ has been verified outside oocytes, using yeast and mammalian cells (28, 41, 46). In the current study, there was H⁺ movement in both acidic Na⁺-containing and acidic Na⁺-free medium, with no significant difference in transport rate between the two conditions. This result indicates that H⁺ is co-transported with uridine in acidic Na⁺-containing buffer. Charge/flux ratio experiments in

oocytes revealed that hCNT3 functions with 2:1 cation:uridine stoichiometry in both acidic and alkaline Na⁺-containing medium, compared with a 1:1 cation:uridine stoichiometry in acidic Na⁺-free medium (10, 12). Because we find similar rates of H⁺ movement in the presence and absence of Na⁺, the present data support a model in which 1 H⁺ and 1 Na⁺ are transported per uridine molecule in acidic Na⁺-containing medium, compared with 1 H⁺ per uridine molecule in the absence of Na⁺, and 2 Na⁺ per uridine molecule in alkaline conditions.

mNect.hCNT3 can be used to measure the transport rate for any nucleoside or nucleoside drug that is co-transported with H⁺, so any range of substrates can be assayed for transport, even if a radioactive analogue is unavailable. This characteristic, along with utilizing a pH-sensitive fluorescent reporter, opens up the possibility of high throughput assays in which a wide range of possible substrates could be added to mNect.hCNT3-transfected cells grown in multiwell plates while monitoring fluorescence changes over time with a multiwell plate fluorometer. mNect.hCNT3 also provides the possibility of high throughput screening for inhibitors, as no high affinity CNT inhibitors have yet been identified. In contrast to hCNT3 assays performed using *X. laevis* oocytes (9, 10, 29), the mNect.hCNT3 assay enables studies of hCNT3 regulation in a physiologically relevant mammalian cell context.

Interestingly, hCNT3 exhibits markedly different selectivity characteristics for symport of physiological nucleosides and therapeutic nucleoside drugs in acidic Na⁺-free or alkaline Na⁺-containing conditions (10). For example, in acidic Na⁺-free conditions, transport of guanosine, 3'-azido-3'-deoxythymidine and 2',3'-dideoxycytidine are almost completely abolished (10, 29). This suggests that binding of Na⁺ or H⁺ induces cation-specific conformational changes in hCNT3 (10). Differential H⁺ or Na⁺ binding to the SGLT1 Na⁺/glucose transporter also leads to cation-specific conformational changes (47). Using mNect.hCNT3, it will be possible to measure transport of nucleosides and nucleoside drugs in acidic Na⁺-containing conditions. In conjunction with corresponding electrophysiological recordings in hCNT3-expressing oocytes (9, 10, 12, 29), it may be possible

mNect.hCNT3 H⁺/Uridine Co-transport

to discern an intermediate conformation where both Na⁺ and H⁺ are bound.

The concentrative nucleoside transporters are primarily expressed in epithelial cells where they are involved in absorption, secretion, distribution, and elimination of nucleosides and nucleoside analogs (2, 3, 11). hCNT3 is especially abundant in the kidney, and may be the key CNT at the apical surface of the proximal tubule (3, 11). The ability of hCNT3 to couple nucleoside movement to either a Na⁺ and/or H⁺ gradient may be advantageous in the kidney, because the lumen of the proximal tubule is acidic, and hCNT3 could take advantage of the H⁺ gradient to maximize its transport rate in these conditions. Both hCNT3 and SGLT1, which have similar transport kinetics, are present in the intestine, which also has an acidic luminal environment, particularly in the more proximal regions (48). Thus, the H⁺-coupling characteristic of hCNT3 may be physiologically and pharmacologically important (3, 9).

The use of pH-sensitive fluorescent protein fusions as an assay of transport activity extends beyond hCNT3. mNectarine could be fused to any transporter that induces a change in intracellular pH. Such transporters could include the H⁺-coupled PepT1/2 peptide transporters (49, 50), SGLT1 (48), and the MCT1 monocarboxylate transporter (51), or any of the transport proteins involved in the regulation of pH_i, including Cl⁻/HCO₃⁻ exchangers (52), NHEs (53), or sodium bicarbonate co-transporters (54). PepT1 (55), MCT1 (56), NHE1 (53), and the SLC4 family members (including Cl⁻/HCO₃⁻ exchangers and sodium bicarbonate co-transporters) (54), all have at least one intracellular terminus, so an mNectarine fusion could be constructed. SGLT1 does not have intracellular N or C termini, but FP fusions could possibly be made in the large cytosolic loop (57). Fusion of mNectarine to these proteins would report on changes in pH local to the transporter and would be more specific than simply measuring pH changes in the bulk cytosol with a pH-sensitive intracellular dye. Moreover, the self-referencing nature of an mNect.transporter fusion ensures that transport activity is measured only in the cells expressing the transport protein. This would be particularly beneficial in studying pH microdomains or metabolons (51, 58).

Furthermore, the spectral characteristics of mNectarine make it ideal for use as a partner with other fluorescent reporters. Even more tantalizing, is the prospect of pairing one mNectarine fusion protein with another pH-sensitive fluorescent protein fusion. This would allow simultaneous measurement of pH in two different regions of a cell. For example, mNectarine can be paired with the green fluorescent protein deGFP4 (15, 59), because they exhibit spectrally distinct wavelengths, which do not exhibit cross-talk (not shown).⁹ Indeed, ongoing studies are investigating the phenomenon of differential pH surrounding pH regulatory transport proteins, resulting from unstirred layer effects.

In conclusion, we have developed a method to measure H⁺/uridine co-transport in mammalian cells by fusing the pH-sensitive fluorescent protein, mNectarine, to the N terminus of hCNT3. mNectarine is a bright, pH-sensitive mRFP with a pK_a

well suited to measurement of physiological pH changes. Fusion to hCNT3 created a self-reporting probe of nucleoside transport that can be expressed in mammalian cells. Furthermore, mNect.hCNT3 reports on nucleoside transport in real-time and enables measurement of the transportability of any substrate that is coupled to H⁺ flux. Fusion to the pH-reporting mNectarine is an approach that could be extended to high throughput assays and could be used to report on the transport activity of any pH transporter. Taken together, our findings demonstrate that mNect.hCNT3 is a valid reporter of H⁺/nucleoside co-transport, and support a transport mechanism where 1 H⁺ and 1 Na⁺ are co-transported with uridine in acidic Na⁺-containing conditions.

Acknowledgments—The cDNA for mCherry2 was kindly provided by Nathan C. Shaner and Roger Y. Tsien (University of California, San Diego).

REFERENCES

- Griffith, D. A., and Jarvis, S. M. (1996) *Biochim. Biophys. Acta* **1286**, 153–181
- Young, J. D., Cheeseman, C. I., Mackey, J. R., Cass, C. E., and Baldwin, S. A. (2000) in *Gastrointestinal Transport (Current Topics in Membranes)* (Barrett, K. E., and Donowitz, M. eds) pp. 329–378, Academic Press, San Diego
- Elwi, A. N., Damaraju, V. L., Baldwin, S. A., Young, J. D., Sawyer, M. B., and Cass, C. E. (2006) *Biochem. Cell Biol.* **84**, 844–858
- King, A. E., Ackley, M. A., Cass, C. E., Young, J. D., and Baldwin, S. A. (2006) *Trends Pharmacol. Sci.* **27**, 416–425
- Zhang, J., Visser, F., King, K. M., Baldwin, S. A., Young, J. D., and Cass, C. E. (2007) *Cancer Metastasis Rev.* **26**, 85–110
- Ritzel, M. W., Yao, S. Y., Huang, M. Y., Elliott, J. F., Cass, C. E., and Young, J. D. (1997) *Am. J. Physiol.* **272**, C707–C714
- Ritzel, M. W., Yao, S. Y., Ng, A. M., Mackey, J. R., Cass, C. E., and Young, J. D. (1998) *Mol. Membr. Biol.* **15**, 203–211
- Ritzel, M. W., Ng, A. M., Yao, S. Y., Graham, K., Loewen, S. K., Smith, K. M., Ritzel, R. G., Mowles, D. A., Carpenter, P., Chen, X. Z., Karpinski, E., Hyde, R. J., Baldwin, S. A., Cass, C. E., and Young, J. D. (2001) *J. Biol. Chem.* **276**, 2914–2927
- Smith, K. M., Slugoski, M. D., Cass, C. E., Baldwin, S. A., Karpinski, E., and Young, J. D. (2007) *Mol. Membr. Biol.* **24**, 53–64
- Smith, K. M., Slugoski, M. D., Loewen, S. K., Ng, A. M., Yao, S. Y., Chen, X. Z., Karpinski, E., Cass, C. E., Baldwin, S. A., and Young, J. D. (2005) *J. Biol. Chem.* **280**, 25436–25449
- Damaraju, V. L., Elwi, A. N., Hunter, C., Carpenter, P., Santos, C., Barron, G. M., Sun, X., Baldwin, S. A., Young, J. D., Mackey, J. R., Sawyer, M. B., and Cass, C. E. (2007) *Am. J. Physiol. Renal Physiol.* **293**, F200–F211
- Slugoski, M. D., Smith, K. M., Mulinta, R., Ng, A. M., Yao, S. Y., Morrison, E. L., Lee, Q. O., Zhang, J., Karpinski, E., Cass, C. E., Baldwin, S. A., and Young, J. D. (2008) *J. Biol. Chem.* **283**, 24922–24934
- Giepmans, B. N., Adams, S. R., Ellisman, M. H., and Tsien, R. Y. (2006) *Science* **312**, 217–224
- Miesenböck, G., De Angelis, D. A., and Rothman, J. E. (1998) *Nature* **394**, 192–195
- Hanson, G. T., McAnaney, T. B., Park, E. S., Rendell, M. E., Yarbrough, D. K., Chu, S., Xi, L., Boxer, S. G., Montrose, M. H., and Remington, S. J. (2002) *Biochemistry* **41**, 15477–15488
- Bizzarri, R., Arcangeli, C., Arosio, D., Ricci, F., Faraci, P., Cardarelli, F., and Beltram, F. (2006) *Biophys. J.* **90**, 3300–3314
- Ai, H. W., Shaner, N. C., Cheng, Z., Tsien, R. Y., and Campbell, R. E. (2007) *Biochemistry* **46**, 5904–5910
- Subach, O. M., Gundorov, I. S., Yoshimura, M., Subach, F. V., Zhang, J., Grünwald, D., Souslova, E. A., Chudakov, D. M., and Verkhusa, V. V. (2008) *Chem. Biol.* **15**, 1116–1124
- Abad, M. F., Di Benedetto, G., Magalhães, P. J., Filippin, L., and Pozzan, T.

⁹ D. E. Johnson, H.-w. Ai, P. Wong, J. D. Young, R. E. Campbell, and J. R. Casey, our observations.

- (2004) *J. Biol. Chem.* **279**, 11521–11529
20. Llopis, J., McCaffery, J. M., Miyawaki, A., Farquhar, M. G., and Tsien, R. Y. (1998) *Proc. Natl. Acad. Sci. U.S.A.* **95**, 6803–6808
21. Matz, M. V., Fradkov, A. F., Labas, Y. A., Savitsky, A. P., Zaraisky, A. G., Markelov, M. L., and Lukyanov, S. A. (1999) *Nat. Biotechnol.* **17**, 969–973
22. Shaner, N. C., Campbell, R. E., Steinbach, P. A., Giepmans, B. N., Palmer, A. E., and Tsien, R. Y. (2004) *Nat. Biotechnol.* **22**, 1567–1572
23. Campbell, R. E., Tour, O., Palmer, A. E., Steinbach, P. A., Baird, G. S., Zacharias, D. A., and Tsien, R. Y. (2002) *Proc. Natl. Acad. Sci. U.S.A.* **99**, 7877–7882
24. Griesbeck, O., Baird, G. S., Campbell, R. E., Zacharias, D. A., and Tsien, R. Y. (2001) *J. Biol. Chem.* **276**, 29188–29194
25. Shaner, N. C., Lin, M. Z., McKeown, M. R., Steinbach, P. A., Hazelwood, K. L., Davidson, M. W., and Tsien, R. Y. (2008) *Nat. Methods* **5**, 545–551
26. Jach, G., Pesch, M., Richter, K., Frings, S., and Uhrig, J. F. (2006) *Nat. Methods* **3**, 597–600
27. Ai, H. W., Henderson, J. N., Remington, S. J., and Campbell, R. E. (2006) *Biochem. J.* **400**, 531–540
28. Zhang, J., Tackaberry, T., Ritzel, M. W., Raborn, T., Barron, G., Baldwin, S. A., Young, J. D., and Cass, C. E. (2006) *Biochem. J.* **394**, 389–398
29. Slugoski, M. D., Ng, A. M., Yao, S. Y., Smith, K. M., Lin, C. C., Zhang, J., Karpinski, E., Cass, C. E., Baldwin, S. A., and Young, J. D. (2008) *J. Biol. Chem.* **283**, 8496–8507
30. Shaner, N. C., Steinbach, P. A., and Tsien, R. Y. (2005) *Nat. Methods* **2**, 905–909
31. Graham, F. L., Smiley, J., Russell, W. C., and Nairn, R. (1977) *J. Gen. Virol.* **36**, 59–74
32. Ruetz, S., Lindsey, A. E., Ward, C. L., and Kopito, R. R. (1993) *J. Cell Biol.* **121**, 37–48
33. Laemmli, U. K. (1970) *Nature* **227**, 680–685
34. Towbin, H., Staehelin, T., and Gordon, J. (1979) *Proc. Natl. Acad. Sci. U.S.A.* **76**, 4350–4354
35. Thomas, J. A., Buchsbaum, R. N., Zimniak, A., and Racker, E. (1979) *Biochemistry* **18**, 2210–2218
36. Sterling, D., and Casey, J. R. (1999) *Biochem. J.* **344**, 221–229
37. Ai, H. W., Olenych, S. G., Wong, P., Davidson, M. W., and Campbell, R. E. (2008) *BMC Biol.* **6**, 13
38. Shu, X., Shaner, N. C., Yarbrough, C. A., Tsien, R. Y., and Remington, S. J. (2006) *Biochemistry* **45**, 9639–9647
39. Hu, H., Endres, C. J., Chang, C., Umapathy, N. S., Lee, E. W., Fei, Y. J., Itagaki, S., Swaan, P. W., Ganapathy, V., and Unadkat, J. D. (2006) *Mol. Pharmacol.* **69**, 1542–1553
40. Plummer, T. H., Jr., and Tarentino, A. L. (1991) *Glycobiology* **1**, 257–263
41. Toan, S. V., To, K. K., Leung, G. P., de Souza, M. O., Ward, J. L., and Tse, C. M. (2003) *Pflugers Arch.* **447**, 195–204
42. Hamilton, S. R., Yao, S. Y., Ingram, J. C., Hadden, D. A., Ritzel, M. W., Gallagher, M. P., Henderson, P. J., Cass, C. E., Young, J. D., and Baldwin, S. A. (2001) *J. Biol. Chem.* **276**, 27981–27988
43. Alexander, R. T., Furuya, W., Szász, K., Orlowski, J., and Grinstein, S. (2005) *Proc. Natl. Acad. Sci. U.S.A.* **102**, 12253–12258
44. Demaurex, N. (2002) *News Physiol. Sci.* **17**, 1–5
45. Chandy, G., Grabe, M., Moore, H. P., and Machen, T. E. (2001) *Am. J. Physiol. Cell Physiol.* **281**, C908–C921
46. Errasti-Murugarren, E., Pastor-Anglada, M., and Casado, F. J. (2007) *J. Physiol.* **582**, 1249–1260
47. Hirayama, B. A., Loo, D. D., and Wright, E. M. (1997) *J. Biol. Chem.* **272**, 2110–2115
48. Hirayama, B. A., Loo, D. D., and Wright, E. M. (1994) *J. Biol. Chem.* **269**, 21407–21410
49. Mackenzie, B., Loo, D. D., Fei, Y., Liu, W. J., Ganapathy, V., Leibach, F. H., and Wright, E. M. (1996) *J. Biol. Chem.* **271**, 5430–5437
50. Chen, X. Z., Zhu, T., Smith, D. E., and Hediger, M. A. (1999) *J. Biol. Chem.* **274**, 2773–2779
51. Becker, H. M., and Deitmer, J. W. (2008) *J. Biol. Chem.* **283**, 21655–21667
52. McMurtrie, H. L., Cleary, H. J., Alvarez, B. V., Loiselle, F. B., Sterling, D., Morgan, P. E., Johnson, D. E., and Casey, J. R. (2004) *J. Enzyme Inhib. Med. Chem.* **19**, 231–236
53. Slepko, E. R., Rainey, J. K., Sykes, B. D., and Fliegel, L. (2007) *Biochem. J.* **401**, 623–633
54. Romero, M. F. (2005) *Curr. Opin Nephrol. Hypertens.* **14**, 495–501
55. Daniel, H., and Kottra, G. (2004) *Pflugers Arch.* **447**, 610–618
56. Poole, R. C., Sansom, C. E., and Halestrap, A. P. (1996) *Biochem. J.* **320**, 817–824
57. Wright, E. M., and Turk, E. (2004) *Pflugers Arch.* **447**, 510–518
58. Sterling, D., Reithmeier, R. A., and Casey, J. R. (2001) *J. Biol. Chem.* **276**, 47886–47894
59. Johnson, D. E., and Casey, J. R. (2008) *FASEB J.* **22**, 759.10 (abstr.)